

**SYNTHESIS OF LARGE PORE ZEOLITES FOR
CATALYZING FURANIC-TYPE FUEL
COMPOUNDS**

NUR HIDAYAHNI BINTI AHMAD

UNIVERSITI SAINS MALAYSIA

2021

**SYNTHESIS OF LARGE PORE ZEOLITES FOR
CATALYZING FURANIC-TYPE FUEL
COMPOUNDS**

by

NUR HIDAYAHNI BINTI AHMAD

**Thesis submitted in fulfilment of the requirement
for the degree of
Doctor of Philosophy**

December 2021

ACKNOWLEDGEMENT

I would like to express my most sincere gratitude to my supervisor, Assoc. Prof. Dr. Ng Eng Poh and my co-supervisor, Prof. Dr. Svetlana Mintova, for their guidance, assistance and encouragement throughout the course of this study. I would also like to acknowledge Pusat Pengajian Sains Kimia, Universiti Sains Malaysia (USM), University of Málaga and Université de Haute Alsace for the facilities provided in order for me to successfully finish this project. I would like to thank research grants (FRGS 203/PKIMIA/6711642 and RUI 1001/PKIMIA/8011128) and my parents for the financial support that allowed me to further my PhD study. Special thanks to all the academic and non-academic staff of the School of Chemical Sciences that have contributed their help throughout my study. I would also like to thank and Global Archeological Research Centre for their assistance in conducting some analyses (FESEM microscopy and XRD measurement). My heartfelt gratitude to my lab mates, Dr. Cynthia, Dr. Tamara, Dr. Ghadah, Dr. Ismail and Dr. Haruna for all their endless guidance, advices and support that helped me in finishing this research. Last but not least, my deepest appreciation is dedicated to my parents and family for their continuous love, support, patience and faith in me. All my accomplishment will not be possible without them in my life.

TABLE OF CONTENTS

ACKNOWLEDGEMENT.....	ii
TABLE OF CONTENTS.....	iii
LIST OF TABLES.....	ix
LIST OF FIGURES.....	xi
LIST OF SYMBOLS, ABBREVIATIONS AND NOMENCLATURES....	xviii
ABSTRAK.....	xxii
ABSTRACT.....	xxiv
CHAPTER 1 INTRODUCTION.....	1
1.1 General introduction.....	1
1.2 Research objectives.....	4
1.3 Overview of the thesis.....	5
CHAPTER 2 LITERATURE REVIEW.....	7
2.1 Zeolites.....	7
2.2 History of zeolites.....	9
2.3 Zeolite synthesis and formation.....	11
2.4 Effect of synthesis parameters on the formation of zeolites.....	15
2.4.1 Source of silica and alumina.....	16
2.4.2 Effect of Si/Al ratio.....	16
2.4.3 Alkalinity.....	17
2.4.4 Effect of water content.....	17
2.4.5 Effect of temperature synthesis.....	18
2.4.6 Effect of synthesis time.....	19

2.4.7	Effect of mineralizing agent.....	19
2.4.8	Effect of structure-directing agents (SDAs).....	20
2.4.9	Effect of gel aging.....	21
2.5	Nanosized zeolites.....	22
2.6	Hierarchical zeolites.....	24
2.7	Linde-type L zeolite (LTL topology).....	27
2.8	Offretite zeolite (OFF topology).....	31
2.9	Zeolites as catalyst.....	36
2.9.1	Dehydration of glucose to 5-hydroxymethylfurfural (5-HMF)...	36
2.9.2	Friedel-Crafts acylation of 2-methylfuran with acetic anhydride	39
2.10	Non-microwave instant heating as a novel heating mode.....	42
CHAPTER 3	MATERIALS AND EXPERIMENTAL	
	METHODS.....	44
3.1	Introduction.....	44
3.2	Chemicals and materials.....	44
3.3	Synthesis of LTL-type zeolites with different morphologies using colloidal HS-40 silica source.....	45
3.4	Synthesis of LTL-type Zeolites with different morphologies using bamboo leaf ash (BLA) silica source.....	47
3.4.1	Preparation of bamboo leaf ash (BLA).....	47
3.4.2	Hydrothermal synthesis of LTL-type zeolites using BLA silica source.....	48
3.5	Synthesis of CTA ⁺ -offretite zeolite.....	50
3.6	Characterizations.....	52
3.6.1	X-ray powder diffraction (XRD) analysis.....	52

3.6.2	Fourier transform infrared (FT-IR) spectroscopy.....	52
3.6.3	Field emission scanning electron microscopy (FESEM).....	53
3.6.4	Solid-state magic-angle spinning nuclear magnetic resonance spectroscopy (MAS NMR).....	53
3.6.5	Inductively coupled plasma-optical emission spectroscopy (ICP-OES).....	54
3.6.6	X-ray fluorescence spectroscopy (XRF).....	54
3.6.7	Nitrogen (N ₂) gas adsorption/desorption analysis.....	54
3.6.8	Thermogravimetry with derivative thermogravimetric (TGA/DTG) analysis.....	55
3.6.9	Temperature-programmed desorption (TPD).....	55
3.6.10	Pyridine adsorption analysis.....	56
3.6.11	High performance liquid chromatography (HPLC) analysis.....	57
3.6.12	Gas chromatography (GC) analysis.....	58
3.6.13	Gas chromatography-mass spectrometry (GC-MS) analysis.....	59
3.7	Catalytic reactions study.....	60
3.7.1	Glucose dehydration.....	60
3.7.2	Acylation of 2-methylfuran with acetic anhydride.....	62
CHAPTER 4	SELECTIVE CONVERSION OF GLUCOSE TO 5-HYDROXYMETHYLFURFURAL BY USING LTL-TYPE ZEOLITES WITH DIFFERENT MORPHOLOGIES.....	64
4.1	Introduction.....	64
4.2	Results and discussion.....	65
4.2.1	Catalyst characterization.....	65

4.2.2	Catalytic reaction study.....	74
4.2.2(a)	Effect of addition of CaCl ₂	75
4.2.2(b)	Reaction temperature dependence and activation energy.....	78
4.2.2(c)	Effect of amount of CaCl ₂ added.....	80
4.2.2(d)	Effect of weight ratio of catalyst loading.....	81
4.2.2(e)	Effect of volume ratio of water and MIBK.....	82
4.2.2(f)	Catalyst reusability study.....	84
4.3	Summary.....	87
CHAPTER 5	MORPHOLOGICAL EFFECTS ON CATALYTIC PERFORMANCE OF LTL ZEOLITES IN ACYLATION OF 2-METHYLFURAN ENHCANCED BY NON-MICROWAVE INSTANT HEATING.....	88
5.1	Introduction.....	88
5.2	Results and discussion.....	89
5.2.1	Characterization of BLA.....	89
5.2.2	Characterization of LTL zeolites.....	92
5.2.3	Catalytic reaction study.....	105
5.2.3(a)	Reaction temperature dependence and activation energy.....	107
5.2.3(b)	Effect of catalyst loading.....	109
5.2.3(c)	Effect of reactants ratio.....	110
5.2.3(d)	Effect of solvents.....	111
5.2.3(e)	Catalyst comparative study.....	112

5.2.3(f)	Catalyst reusability study.....	113
5.3	Summary.....	115
CHAPTER 6	SYNTHESIS OF OFFRETITE ZEOLITE SINGLE CRYSTALS USING AMPHIPHILE-TEMPLATING APPROACH AND ITS CATALYTIC PERFORMANCE.....	116
6.1	Introduction.....	116
6.2	Results and discussion.....	117
6.2.1	Effect of synthesis parameters on the synthesis of OFF zeolite....	117
6.2.1(a)	Effect of crystallization temperature.....	117
6.2.1(b)	Effect of crystallization time.....	120
6.2.1(c)	Effect of SiO ₂ /Al ₂ O ₃ ratio.....	122
6.2.1(d)	Effect of CTABr content.....	124
6.2.1(e)	Effect of mineralizer.....	126
6.2.1(f)	Effect of H ₂ O content.....	129
6.2.2	Characterization of OFF zeolite (SF3).....	131
6.2.3	Catalytic reaction studies.....	134
6.2.3(a)	Effect of reaction temperature and time.....	135
6.2.3(b)	Effect of catalyst loading.....	137
6.2.3(c)	Effect of reactants ratio.....	138
6.2.3(d)	Effect of solvents.....	139
6.2.3(e)	Catalyst comparative study.....	140
6.2.3(f)	Catalyst reusability study.....	141
6.3	Conclusion.....	142

CHAPTER 7	CONCLUSION AND RECOMMENDATIONS.....	144
7.1	Conclusion.....	144
7.2	Recommendation of future works.....	145
	REFERENCES.....	147
	APPENDICES	
	LIST OF PUBLICATIONS AND OTHERS	

LIST OF TABLES

		Page
Table 2.1	A summary of the main effects of hierarchical zeolites in various catalytic petrochemical reactions [103].....	27
Table 2.2	The synthesis conditions of LTL zeolite with various morphologies and crystal sizes.....	30
Table 2.3	The synthesis conditions of OFF zeolite using different types of SDAs and the obtained final crystalline products.....	35
Table 2.4	Dehydration of glucose to 5-HMF reaction catalysed using various solid acid catalyst under different conditions.....	39
Table 2.5	Catalytic activities of various reported catalysts in acylation of 2-methylfuran with acetic anhydride.....	41
Table 3.1	Experimental conditions for the synthesis of LTL-type zeolites with different morphologies.....	47
Table 3.2	Molar compositions of hydrogels and the synthesis conditions for the preparation of LTL zeolites.....	49
Table 3.3	Synthesis conditions for studying the effects of synthesis variables on crystallization of OFF zeolite.....	51
Table 3.4	HPLC instrument setup for studying catalytic reactions.....	58
Table 3.5	GC oven-programmed setup for studying catalytic reactions.....	59
Table 4.1	ICP-OES data of LTL zeolites.....	67
Table 4.2	Textural and acid properties of LTL zeolites.....	68
Table 4.3	Surface acidity of zeolite LTL with different morphologies at different temperatures.....	74
Table 5.1	ICP-OES analysis of BLA after acid treatment.....	90

Table 5.2	Chemical compositions, surface and textural properties of LTL zeolites.....	96
Table 5.3	Characterization of surface acidity of zeolites LTL with various morphologies.....	103
Table 5.4	Effect of solvent on Friedel-Crafts acylation of 2-methylfuran reaction. ^a	112
Table 6.1	Properties of offretite zeolites.....	132
Table 6.2	Effect of solvent on Friedel-Crafts acylation of 2-methylfuran reaction. ^a	140

LIST OF FIGURES

		Page
Figure 2.1	The formation of zeolite framework by of silica (SiO_4) and alumina (AlO_4) tetrahedra, where the metal cation (M^+) neutralizes the negative charged of aluminosilicate framework.....	7
Figure 2.2	(a) Primary building units (PBUs), (b) secondary building units (SBUs), (c) tertiary units or composite building units (CBUs) and (d) zeolite structures [37].....	9
Figure 2.3	The hydrothermal process of zeolite synthesis.....	13
Figure 2.4	Schematic representation of the (a) nucleation and (b) crystal growth rate of zeolites, and (c) formation of zeolite from amorphous particles during the synthesis [56].....	15
Figure 2.5	The properties of nanosized zeolites [3].....	22
Figure 2.6	Synthesis parameters affecting the formation of zeolite nanocrystals [92].....	23
Figure 2.7	The synthesis methods of nanosized zeolites [92].....	24
Figure 2.8	Diagram of different molecular diffusion pathways (A, B and C) for conventional and hierarchical micro/mesoporous zeolites where the hierarchical zeolites show shorter diffusion pathways (A and C) than the conventional zeolites [103].....	25
Figure 2.9	Various synthesis routes of micro/mesoporous zeolite materials [107].....	26
Figure 2.10	SBUs and composite building units of LTL framework: (a) 4-2 unit, (b) 6-ring, (c) double-6-ring (D6R), (d) cancrinite cage and (e) double sawtooth chain (<i>dsc</i>), that result in (f) the formation of 12-membered ring channel system (viewed along [001] plane) [109].....	28
Figure 2.11	SBUs and composite building units of OFF framework: (a) 4-2 units and (b) 6-rings; and (c) double-6-ring (D6R), (d) <i>can</i> cage, (e) <i>gme</i> cavities and (f) double sawtooth chain (<i>dsc</i>), respectively [109].....	32

Figure 2.12	The (a) <i>can</i> cages, (b) <i>gme</i> cavities and (c) 12-ring channel seen along $\langle 120 \rangle$ in OFF framework structure [109].....	33
Figure 2.13	The 12-membered ring and 8-membered ring channel system in OFF-type zeolite viewed along [001] [109].....	33
Figure 2.14	Reaction pathway of glucose to 5-hydroxymethylfurfural.....	37
Figure 2.15	Reaction pathway of 2-methylfuran with acetic anhydride to form 2-acetyl-5-methylfuran.....	40
Figure 2.16	Schematic drawing depicting the concept of a conductively heated sealed vial reactor employing a 10 mL glass vial [154]..	43
Figure 2.17	Anton Paar's Monowave 50 with open cover and 10-mL glass vials [154].....	43
Figure 3.1	The procedure flow for the hydrothermal synthesis of LTL zeolite.....	46
Figure 3.2	The schematic procedure for the preparation of amorphous bamboo leaf ash (BLA).....	48
Figure 3.3	The schematic scheme for the hydrothermal synthesis of LTL zeolite using BLA.....	50
Figure 3.4	The schematic flow for the hydrothermal synthesis of OFF zeolite using CTABr as SDA.....	52
Figure 4.1	(a) Structure of zeolite LTL view along [001] plane illustrating its hexagonal framework. (b) An LTL channel view normal to [001] plane that consists of 0.71 nm unit cells with a pore opening of 0.71 nm. (c) Schematic illustration of diffusion of glucose as reactant and HMF as product in the 12-membered ring channel of LTL zeolite.....	65
Figure 4.2	XRD patterns of (a) ROD-LTL, (b) NEEDLE-LTL and (c) CYL-LTL zeolites.....	66
Figure 4.3	(A) N ₂ adsorption-desorption isotherms and (B) pore size distributions of LTL zeolites at -196 °C of (a) ROD-LTL, (b) NEEDLE-LTL and (c) CYL-LTL zeolites.....	69
Figure 4.4	SEM images and particle size distribution histograms of LTL-zeolite crystals synthesized of (a) ROD-LTL, (b) NEEDLE-LTL and (c) CYL-LTL.....	71
Figure 4.5	²⁷ Al Solid state nuclear magnetic resonance spectra of (a) NEEDLE-LTL, (b) ROD-LTL and (c) CYL-LTL zeolites....	72

Figure 4.6	NH ₃ desorption of LTL-based zeolites as a function of the strength: weak (100-200 °C), medium (200-300 °C) and strong (300-550 °C).....	73
Figure 4.7	Effect of the addition of CaCl ₂ on the catalytic performance. Reaction temperature = 150 °C, time = 60 min, catalyst = 0.05 g, glucose = 0.15 g, water = 1.5 mL, MIBK = 3.5 mL, CaCl ₂ = 0.65 g g _{H₂O} ⁻¹	76
Figure 4.8	The glucose conversion and 5-HMF yield (dark grey line = CaCl ₂ , dark yellow line = CaCl ₂ /NEEDLE-LTL) of CaCl ₂ and CaCl ₂ /NEEDLE-LTL. Reaction temperature = 150 °C, catalyst (NEEDLE-LTL) = 0.05 g, glucose = 0.15 g, water = 1.5 mL, MIBK = 3.5 mL, CaCl ₂ = 0.65 g g _{H₂O} ⁻¹	77
Figure 4.9	Kinetics of glucose dehydration ((A) glucose conversion at 150 °C; (B) 5-HMF yield at 150 °C; (C) glucose dehydration at 175 °C; (D) 5-HMF yield at 175 °C) for (a) ROD-LTL, (b) NEEDLE-LTL and (c) CYL-LTL zeolites. Catalyst = 0.05 g, glucose = 0.15 g, water = 1.5 mL, MIBK = 3.5 mL, CaCl ₂ = 0.65 g g _{H₂O} ⁻¹	79
Figure 4.10	The Arrhenius plots for (a) ROD-LTL, (b) NEEDLE-LTL and (c) CYL-LTL zeolite catalysts. Catalyst = 0.05 g, glucose = 0.15 g, water = 1.5 mL, MIBK = 3.5 mL, CaCl ₂ = 0.65 g g _{H₂O} ⁻¹	80
Figure 4.11	Influence of the CaCl ₂ content with NEEDLE-LTL (Experimental conditions: 0.15 g glucose, 0.05 g catalyst, 1.5 mL water, 3.5 mL MIBK, Temperature: 175 °C; time: 120 min).....	81
Figure 4.12	Influence of the glucose:catalyst (NEEDLE-LTL) weight ratio. Reaction temperature = 150 °C, time = 60 min, glucose = 0.15 g, water = 1.5 mL, MIBK = 3.5 mL, CaCl ₂ = 0.65 g g _{H₂O} ⁻¹	82
Figure 4.13	Effect of the volume ratio of water:MIBK with NEEDLE-LTL. Reaction temperature = 170 °C, time = 120 min, catalyst (NEEDLE-LTL) = 0.05 g, glucose = 0.15 g, water = 1.5 mL, CaCl ₂ = 0.65 g g _{H₂O} ⁻¹	83

Figure 4.14	Reusing study of NEEDLE-LTL after (1) drying at 65 °C, (2) washing with water/acetone. Reaction temperature = 150 °C, time = 60 min, catalyst (NEEDLE-LTL) = 0.05 g, glucose = 0.15 g, water = 1.5 mL, MIBK = 3.5 mL, CaCl ₂ = 0.65 g g _{H₂O} ⁻¹	85
Figure 4.15	TGA curves of (a) fresh and (b) used (glucose:catalyst weight ratio = 1:1, T = 150 °C, time = 60 min) NEEDLE-LTL zeolite.....	86
Figure 5.1	XRD pattern of BLA.....	90
Figure 5.2	FTIR spectrum of BLA.....	91
Figure 5.3	TGA-DTG curves of BLA.....	92
Figure 5.4	(a) View of LTL zeolite framework along [001] plane showing its hexagonal structure; (b) schematic illustration of diffusion of reactants (2-methylfuran and acetic anhydride) and product (2-acetyl-5-methylfuran) in the LTL channel with a van der Waals opening of 7.1 Å and a maximum internal pore diameter of 1.26 Å.....	93
Figure 5.5	XRD patterns of (a) theoretical, (b) cylindrical, (c) stick-like, (d) short-rod and (e) nanosized LTL zeolites.....	94
Figure 5.6	SEM images of (a) cylindrical, (b) stick-like and (c) short-rod LTL zeolites, and (d) nanosized LTL zeolite.....	95
Figure 5.7	IR spectra of (a) cylindrical, (b) stick-like, (c) short-rod and (d) nanosized LTL zeolites.....	98
Figure 5.8	(A) TGA and (B) DTG plots of (a) cylindrical, (b) stick-like, (c) short-rod and (d) nanosized LTL zeolites.....	99
Figure 5.9	Nitrogen gas adsorption-desorption isotherms of (a) cylindrical, (b) stick-like, (c) short-rod and (d) nanosized LTL zeolites. Inset: Pore size distributions derived from DFT model.....	101
Figure 5.10	TPD-NH ₃ curves of (a) cylindrical, (b) stick-like, (c) short-rod and (d) nanosized LTL zeolites.....	105

Figure 5.11	Effect of temperature and time on the conversion at (A) 140 °C, (B) 150 °C and (C) 160 °C for (a) cylindrical, (b) stick-like, (c) short-rod and (d) nanosized LTL zeolites. (D) The Arrhenius plots of the LTL zeolite catalysts. Catalyst = 0.30 g, 2-methylfuran = 4.7 mmol, acetic anhydride = 14.1 mmol, solvent-free.....	106
Figure 5.12	Percentage conversion of 2-methylfuran at different amount of catalyst (nanosized LTL). Reaction temperature = 160 °C, time = 20 min, 2-methylfuran = 4.7 mmol, acetic anhydride = 14.1 mmol, solvent-free.	110
Figure 5.13	Percentage conversion of 2-methylfuran at different 2-methylfuran:acetic anhydride molar ratios. Reaction conditions: temperature = 160 °C, time = 20 min, catalyst (nanosized LTL) = 0.3 g, solvent-free.....	111
Figure 5.14	Conversion of 2-methylfuran versus types of catalysts. Reaction conditions: temperature = 160 °C, time = 20 min, 2-methylfuran = 4.7 mmol, acetic anhydride = 14.1 mmol, catalyst = 0.30 g (or equivalent to 0.1148 mmol), solvent-free.....	113
Figure 5.15	Reusability test of nanosized LTL zeolite. Reaction conditions: temperature = 160 °C, time = 20 min, 2-methylfuran = 4.7 mmol, acetic anhydride = 14.1 mmol, catalyst (nanosized LTL) = 0.30 g, solvent-free.....	114
Figure 6.1	(A) XRD patterns and (B) FESEM images of (a) SF1, (b) SF2 and (c) SF3 samples prepared with a hydrogel molar composition of 20SiO ₂ :1Al ₂ O ₃ :1.46CTABr:10K ₂ O:800H ₂ O and heated at 140 °C, 160 °C and 180 °C heated for 72 h, respectively.....	119
Figure 6.2	(A) XRD patterns and (B) FESEM images of (a) SF4, (b) SF5, (c) SF6 and (d) SF3 solids prepared with a hydrogel containing 20SiO ₂ :1Al ₂ O ₃ :1.46CTABr:10K ₂ O:800H ₂ O and heated at 180 °C for 40 h, 55 h, 65 h and 72 h, respectively. Notes: O = OFF, M = MER and L = LTL phases.....	121
Figure 6.3	(A) XRD patterns and (B) FESEM images of (a) SF7 (<i>w</i> = 10), (b) SF8 (<i>w</i> = 12), (c) SF9 (<i>w</i> = 15) and (d) SF3 (<i>w</i> = 20) where the samples were obtained using precursor hydrogels of <i>w</i> SiO ₂ :1Al ₂ O ₃ :1.46CTABr:10K ₂ O:800H ₂ O at 180 °C heated for 72 h. Notes: L = LTL, P = PHI, U = unknown phase.....	123

Figure 6.4	(A) XRD patterns and (B) FESEM images of (a) SF10 ($x = 0$), (b) SF11 ($x = 1.35$), (c) SF3 ($x = 1.46$) and (d) SF12 ($x = 1.83$) where the powder samples were prepared using precursor hydrogels containing $20\text{SiO}_2:1\text{Al}_2\text{O}_3:x\text{CTABr}:10\text{K}_2\text{O}:800\text{H}_2\text{O}$ at $180\text{ }^\circ\text{C}$ heated for 72 h.....	125
Figure 6.5	(A) XRD patterns and (B) FESEM images of (a) SF13 ($y = 2.5$), (b) SF14 ($y = 7.5$), (c) SF3 ($y = 10$) and (d) SF15 ($y = 12.5$) where the powder samples were obtained using hydrogels of $20\text{SiO}_2:1\text{Al}_2\text{O}_3:1.46\text{CTABr}:y\text{K}_2\text{O}:800\text{H}_2\text{O}$ at $180\text{ }^\circ\text{C}$ heated for 72 h.....	127
Figure 6.6	(A) XRD patterns and (B) FESEM images of (a) SF16, (b) SF3 and (c) SF17. The powder samples were obtained by heating the precursor hydrogel of $20\text{SiO}_2:1\text{Al}_2\text{O}_3:1.46\text{CTABr}:10\text{M}_2\text{O}:800\text{H}_2\text{O}$ at $180\text{ }^\circ\text{C}$ heated for 72 h, where $\text{M} = \text{Na}^+, \text{K}^+$ and Cs^+ , respectively.....	128
Figure 6.7	(A) XRD patterns and (B) FESEM images of (a) SF16 ($z = 600$), (b) SF3 ($z = 800$), (c) SF17 ($z = 1000$) and (d) SF18 ($z = 1200$) where the powder samples were obtained using precursor hydrogels containing a composition of $20\text{SiO}_2:1\text{Al}_2\text{O}_3:1.46\text{CTABr}:y\text{K}_2\text{O}:800\text{H}_2\text{O}$ heated at $180\text{ }^\circ\text{C}$ for 72 h.....	130
Figure 6.8	Nitrogen adsorption-desorption isotherms (inset: pore size distributions) of (a) $\text{CTA}^+\text{-OFF}$ (SF3) and (b) $\text{TMA}^+\text{-OFF}$ zeolites.....	131
Figure 6.9	Formation mechanism of OFF zeolite templated by CTA^+ cation. K atoms are not shown for simplicity.....	133
Figure 6.10	$\text{NH}_3\text{-TPD}$ profiles of (a) $\text{CTA}^+\text{-OFF}$ (SF3) and (b) $\text{TMA}^+\text{-OFF}$ zeolites.....	134
Figure 6.11	Effect of temperature and time on the conversion at (a) $150\text{ }^\circ\text{C}$, (b) $160\text{ }^\circ\text{C}$ and (c) $170\text{ }^\circ\text{C}$. Catalyst = 0.30 g, 2-methylfuran = 4.7 mmol, acetic anhydride = 14.1 mmol, solvent-free.....	136
Figure 6.12	The Arrhenius plots of the acylation reaction with and without OFF zeolite catalyst. Catalyst = 0.30 g, 2-methylfuran = 4.7 mmol, acetic anhydride = 14.1 mmol, solvent-free.....	137

Figure 6.13	Percentage conversion of 2-methylfuran at different amounts of OFF zeolite catalyst. Reaction temperature = 170 °C, time = 40 min, 2-methylfuran = 4.7 mmol, acetic anhydride = 14.1 mmol, solvent-free.....	138
Figure 6.14	Percentage conversion of 2-methylfuran at different 2-methylfuran:acetic anhydride molar ratios. Reaction conditions: temperature = 170 °C, time = 40 min, catalyst = 0.3 g, solvent-free.....	139
Figure 6.15	Conversion of 2-methylfuran versus types of catalysts. Reaction conditions: temperature = 170 °C, time = 40 min, 2-methylfuran = 4.7 mmol, acetic anhydride = 14.1 mmol, catalyst = 0.30 g (or equivalent to 0.20 mmol), solvent-free...	141
Figure 6.16	Reusability test of OFF zeolite. Reaction conditions: temperature = 170 °C, time = 40 min, 2-methylfuran = 4.7 mmol, acetic anhydride = 14.1 mmol, catalyst = 0.30 g, solvent-free.....	142

LIST OF SYMBOLS, ABBREVIATIONS AND NOMENCLATURES

°	Degree
α	Alpha
β	Beta
γ	Gamma
λ	Lambda
θ	Theta
°C	Degree Celsius
μm	Micrometer
Å	Angstrom (= 10^{-10} meters)
(H-[Al]-Beta)	Lewis acid Beta zeolites
(H-[Al]-Beta)	Brönsted acid Beta zeolite
Al	Aluminum
Al^{3+}	Aluminum cation
AlO_4	Aluminum tetraoxide
Al_2O_3	Aluminum oxide
$\text{Al}(\text{OH})_3$	Aluminum hydroxide
ANA	Analcime
BET	Brunauer-Emmet-Teller
BLA	Bamboo leaf ash
C	Carbon
ca.	Approximately

Cs	Cesium
cm	Centimeter
CO ₂	Carbon dioxide
D4R	Double four rings
D6R	Double six rings
D8R	Double eight rings
DMSO	Dimethyl sulfoxide
DTG	Derivative thermogravimetry
d _z	Average diameter of zeolite crystals in nm
e.g.	Example
E _T ^N	Empirical solvent polarities
F ⁻	Fluoride ion
FESEM	Field emission scanning electron microscopy
FeCl ₃	Iron (III) chloride
FT-IR	Fourier transform infrared spectroscopy
g	Gram
GC	Gas chromatography
h	Hour
H ⁺	Proton
H ₂ O	Water
HCl	Hydrochloric acid
HF	Hydrofluoric acid
HMF	Hydroxymethylfurfural

HNO ₃	Hydrofluoric acid
ICP-OES	Inductively coupled plasma-optical emission spectroscopy
IUPAC	International Union of Pure and Applied Chemistry
IZA-SC	International Zeolite Association Structure Commission
kHz	Kilohertz
kV	Kilovolt
K ⁺	Potassium cation
KBr	Potassium bromide
K ₂ O	Potassium oxide
KOH	Potassium hydroxide
LTL	Linde-type L
m/z	Mass to charge ratio
M	Molarity
MAS NMR	Magic angle spinning nuclear magnetic resonance
mbar	Milibar
min	Minute
mL	Millilitre
mm	Millimetre
mmol	millimol
MS	Mass spectrometry
n _{ch}	Number of parallel channels
N ₂	Nitrogen molecule
Na ⁺	Sodium cation
NH ₃	Ammonia

Na ₂ O	Sodium oxide
nm	Nanometer
OH ⁻	Hydroxide ion
OFF	Offretite
OSDA	Organic structure-directing agent
PBU	Primary building unit
ppm	Part per million
rpm	Revolutions per minute
SBU	Secondary building unit
SDA	Structure-directing agent
Si	Silicon
SiO ₂	Silicon dioxide
t	Time
T	Temperature
<i>T</i>	Transmittance
TCD	Thermal conductivity detector
TEAOH	Tetraethylammonium hydroxide
TEOS	Tetraethylorthosilicate
TGA	Thermogravimetry analysis
TPD	Temperature programmed desorption
wt.%	Weight percentage
XRD	X-ray diffraction
ZnCl ₂	Zinc chloride

SINTESIS ZEOLIT BERLIANG BESAR UNTUK PEMANGKINAN SEBATIAN BAHAN API BERASASKAN FURAN

ABSTRAK

Zeolit jenis Linde L (topologi LTL) dan offretit (topologi OFF) adalah zeolit berliang besar (masing-masing berdiameter $7.1 \times 7.1 \text{ \AA}^2$ dan $6.7 \times 6.8 \text{ \AA}^2$). Objektif projek ini adalah untuk mensistesis and menggunakan mangkin asid zeolit LTL dan OFF dalam memangkinakan pelbagai tindak balas berasaskan furan. Bahagian pertama memberi tumpuan kepada kajian kesan morfologi terhadap sifat keliangan dan keasidan permukaan zeolit LTL dan prestasi pemangkinannya. Didapati zeolit LTL dengan keasidan, saiz zarah dan morfologi (jarum, rod pendek dan silinder) yang berlainan telah berjaya disintesis dengan menggunakan kaedah hidrotermal dan zeolit LTL berbentuk jarum memberi prestasi pemangkinan tertinggi dalam sintesis 5-hidroksimetilfurfural (5-HMF), dengan 88% penukaran glukosa dan 63% hasil 5-HMF pada suhu $175 \text{ }^\circ\text{C}$ selepas 90 min tindak balas. Bahagian kedua fokus kepada kesan morfologi zeolit LTL (rod pendek, silinder, batang dan nanosaiz) terhadap pengasilan 2-metilfuran dengan asetik anhidrida dan abu daun buluh (BLA) digunakan sebagai sumber silika. Pada $160 \text{ }^\circ\text{C}$ selama 20 min tindak balas, zeolit LTL nanohablur merupakan mangkin asid pepejal yang terbaik dalam pengasilan 2-metilfuran (97.2% penukaran, 100% selektif terhadap 2-asetil-5-metilfuran) disebabkan tapak asidnya yang mudah dicapai. Akhir sekali, kesan reaktan hydrogel dan parameter sintesis (seperti suhu pemanasan dan masa tindak balas) terhadap penghabluran zeolit OFF dikaji. Didapati komposisi kimia reaktan dan keadaan sintesis mempunyai kesan tersendiri terhadap kadar penghabluran, ketulenan fasa dan morfologi zeolit OFF. Zeolit OFF tulen dengan keliangan hierarki dapat dihablurkan menggunakan hidrogel

berkomposisi $20\text{SiO}_2:1\text{Al}_2\text{O}_3:1.46\text{CTABr}:10\text{K}_2\text{O}:800\text{H}_2\text{O}$ pada suhu $180\text{ }^\circ\text{C}$ selama 72 jam. Ia juga menunjukkan zeolit OFF mencapai prestasi pemangkinan yang tinggi (82.3% penukaran, 100% selektif kepada 2-asetil-5-metilfuran) dalam tindak balas pengasilan Friedel-Crafts 2-metilfuran dengan asetik anhidrida dalam keadaan pemanasan segera bukan gelombang mikro ($170\text{ }^\circ\text{C}$, 40 min). Secara kesimpulan, zeolit LTL dan OFF telah berjaya disintesis dan kedua-duanya menunjukkan potensi sebagai mangkin heterogen dalam tindak balas berasaskan furan.

SYNTHESIS OF LARGE PORE ZEOLITES FOR CATALYZING FURANIC- TYPE FUEL COMPOUNDS

ABSTRACT

Linde type L (LTL topology) and offretite (OFF topology) zeolites are large pore zeolites (diameter $7.1 \times 7.1 \text{ \AA}^2$ and $6.7 \times 6.8 \text{ \AA}^2$, respectively). The aim of this project is to synthesize and apply LTL and OFF acidic zeolites in catalyzing various furanic-type reactions. The first part focuses on studying the effects of morphology on porous properties and surface acidity of LTL zeolites and its catalytic performance. It is found that the LTL zeolites with different acidities, particle sizes and morphologies (needle, short rod, and cylinder) was successfully synthesized using hydrothermal method where LTL zeolite with needle shape gives the highest catalytic performance in the synthesis of 5-hydroxymethylfurfural (5-HMF), having 88% glucose conversion and 63% 5-HMF yield at 175 °C after 90 min of reaction. The second part studies the morphological effects of LTL zeolites (short-rod, cylindrical, stick-like and nanosized) on the acylation of 2-methylfuran with acetic anhydride where bamboo leave ash is used as silica source. At 160 °C for 20 min of reaction, nanosized LTL zeolite is the best solid acid catalyst in the acylation of 2-methylfuran (97.2% conversion, 100% selective to 2-acetyl-5-methylfuran) due to its high accessible acid sites. Lastly, the effects of initial precursor hydrogel and synthesis parameters (e.g. heating temperature and reaction time) on the crystallization of OFF zeolite are explored. It is shown that the reactant chemical composition and synthesis conditions have independent effects on the crystallization rate, phase purity, crystal size and morphology of OFF zeolite. Pure OFF zeolite with hierarchical porosity is crystallized using a hydrogel of a composition of $20\text{SiO}_2:1\text{Al}_2\text{O}_3:1.46\text{CTABr}:10\text{K}_2\text{O}:800\text{H}_2\text{O}$ at 180 °C for 72 h. It also

shows that the OFF zeolite has high catalytic performance (82.3% conversion, 100% selective to 2-acetyl-5-methylfuran) in Friedel-Crafts acylation reaction of 2-methylfuran with acetic anhydride under non-microwave instant heating conditions (170 °C, 40 min). In conclusion, LTL and OFF zeolites have successfully been synthesized and both show promising as heterogenous catalysts in furanic-type reactions.

CHAPTER ONE

INTRODUCTION

1.1 General introduction

Zeolites are microporous crystalline aluminosilicates composed of silica (SiO_4) and alumina (AlO_4) tetrahedra with O atoms connecting the neighbouring tetrahedral to form three-dimensional open structures such as channels and cavities. The combination of SiO_4 units forms silica (SiO_2), which is a neutral solid. By incorporating aluminum (Al) into it, the Al^{3+} makes the framework to be negatively charge. In order to neutralize the overall framework, the non-framework cations are needed to counter-balance the framework charge, creating a strong electrostatic field on the zeolite's surface [1,2]. Zeolites are very stable, resistant to high temperature and pressure, high porosity, tunable acidity/basicity and high ion-exchange capacity. Because of these features synthetic zeolites have a broad range of industrial, commercial and consumer uses, such as catalysis, ion exchange, adsorption and separation processes [1,2].

Nanosized particles with a crystallite size in the range of 5–100 nm has been a great interest in materials research due to their increase in external surface area that enhance their properties. These surface properties overcome the limitation of adsorption of bulky molecules. Due to the unique properties, nanosized zeolites are used in many aspects including catalysis, lubricants, sensing, adsorption and so on [3].

Hierarchical porous materials are another material that has gained a lot of interest recently due to various porosity (micro-, meso- and macropores) [4,5].

Mesopores (2-50 nm) and macropores overcomes the limitation diffusion and accessibility of large molecules. Hierarchical zeolite have many potential application such as catalysts for hydrocracking, alkylation, esterification, olefin aromatization and methanol to hydrocarbons (MTH) conversion reactions [6-13].

Linde-type zeolite (LTL) is a large-pore zeolite consisting of 12-ring channels was first synthesized by Breck and Flanigen in 1965 [14]. Zeolite LTL is applied in variety of applications such as host-guest composites, sorbent, catalyst, membrane, ion-exchange and separations, fuel upgrading and production of petrochemical intermediates due to their large-pore properties that allows ease molecular diffusion and accessibility [15-17]. The type of silica sources used can influence the overall zeolite products such as the particle size and crystal morphology. The commonly used silica sources are silica sol, sodium silicate and colloidal silica. However, over the years there is an increase interest on the synthesizing of zeolite using agricultural wastes such as bamboo leaves ash (BLA) as silica source. Compared to other conventional silica source, BLA is considered as a cheap, eco-friendly and highly active silica source. The design of cheaper, less toxic, less corrosive and reusable zeolites using agricultural waste as silica source are highly preferable for a green chemistry approach. Zeolite LTL with different crystal sizes and morphologies can be synthesized by modifying the chemical composition of the starting hydrogel precursor ($\text{SiO}_2/\text{Al}_2\text{O}_3$ ratio, KOH and water content) and the synthesis parameters (crystallization time and temperature). Nevertheless, there is a lack of study in the morphology effects on the porous properties and surface acidity of LTL zeolites synthesized using colloidal silica and BLA as silica source.

Offretite zeolite (OFF) consisting of 12-membered ring windows and a hexagonal crystal structure was first described by Gonnard in 1890 [18]. Due to its large pore channels with 12-membered ring size with diameter $6.7 \times 6.8 \text{ \AA}^2$, OFF zeolite has been selected as a selective catalyst for various industrial processes, including methanol-to-olefin reaction, paraffin cracking and separation [19-22]. OFF zeolite is typically synthesized using tetramethylammonium (TMA^+) as an organic structure-directing agent (SDA) in the presence of both NaOH and KOH mineralizers. However, the formation of OFF zeolite is seldom crystallized completely free from erionite (ERI) zeolite intergrowth and only crystals with microporosity are produced. The synthesis of hierarchical porous OFF zeolite with high purity and facile synthesis approach still remains a challenge.

In recent years, attention is also paid to the development of eco-friendly and cheaper synthetic techniques for synthesizing chemicals from non-fossil carbon sources [23]. The hydrolysis of cellulose and hemicellulose leads to monomeric C_5 and C_6 sugars, which can be converted into important platform molecules, such as furfural and 5-hydroxymethylfurfural (5-HMF), respectively, which are the starting point for the synthesis of a large variety of biofuels and chemicals [24,25]. The global furfural market size was valued at \$1.2 billion in 2019 and is anticipated to generate \$2.0 billion by 2027, with an experience growth at a CAGR of 6.9% from 2020 to 2027 [26]. Meanwhile, the global 5-hydroxymethylfurfural (5-HMF) market is valued at \$55,867 in 2018 and is expected to reach \$62,700 by the end of 2025, growing at a CAGR of 1.45% between 2018 and 2025 [27]. Although the dehydration of fructose to 5-HMF has largely been reported in the literature [28-31], glucose is preferred due to its abundance and low price [32]. Homogeneous catalysts such as sulphuric or hydrochloric acids are generally used for the hydrolysis of cellulose to glucose or

dehydration of fructose to 5-HMF. However, due to their corrosive properties heterogeneous catalysts are much preferred nowadays.

Friedel-Crafts acylation reactions are traditionally catalyzed by Lewis acids such as zinc chloride, aluminum trichloride, iron(III) trichloride, tin(IV) tetrachloride and titanium(IV) tetrachloride, or strong protic acids like hydrofluoric acid and sulfuric acid [33]. However, these homogenous catalysts are harmful, corrosive, less selective and difficult to reuse. During the past decades, the development of more environmentally and effective acylation process has become a goal in organic synthesis [34]. Furan and its acylated derivatives are important aromatic compounds that are widely used in drug, food, fragrance, petrochemical and fine chemical industries. The reaction of interest in this research is the acylation of 2-methylfuran with acetic anhydride. The product obtained is 2-acetyl-5-methylfuran which is a valuable biofuel and intermediate in pharmaceutical industry [30]. The roles of zeolite morphology on dehydration of glucose and Friedel Crafts acylation of 2-methylfuran reaction are still unclear. Also, there is a lack of study for hierarchical OFF zeolite performance in these catalytic reactions.

1.2 Research objectives

The objectives of this research are:

1. To synthesize and characterize LTL zeolites using colloidal silica and bamboo leaves ash (BLA) as silica sources.
2. To correlate the effects of morphological properties on the porous properties and surface acidity properties of LTL zeolites.

3. To study the effects of initial reactants and synthesis conditions on the crystallization of OFF zeolite (crystallization kinetics, crystalline phase, morphology, topology) templated by cetyltrimethylammonium bromide.
4. To investigate the catalytic performance of LTL and OFF zeolites in furanic reactions, namely dehydration of glucose to 5-hydroxymethylfurfural (5-HMF) and acylation of 2-methylfuran with acetic anhydride under non-microwave instant heating conditions.

1.3 Overview of the thesis

This thesis is composed of seven chapters which covers the project background, literature study, experimental procedures, and research findings of the project. Chapter One presents a general introduction of the research, the problem statements and research objectives of the project. Chapter Two details the literature review focusing on the background and history of zeolites, zeolite synthesis, zeolite formation and parameters affecting the formation of zeolites, nanosized zeolite, hierarchical zeolites, application of zeolite particularly as a heterogenous catalyst, and the catalytic reactions chosen for this project.

Chapter Three describes the research methodologies that were carried out throughout the whole project, including the hydrothermal synthesis of LTL zeolite with different morphologies using colloidal silica and bamboo leaf ash (BLA) as silica sources, the study of effects of synthesis parameters on the formation of OFF zeolite using cetyltrimethylammonium bromide (CTABr) as structure-directing agent (SDA), the characterization techniques used and the catalytic performance study for LTL and OFF zeolites.

Chapter Four reports the synthesis and characterization of LTL zeolite with different morphologies (needle, short rod, cylinder) using colloidal silica as silica source. The relationship between crystal morphologies and their catalytic performance were then investigated in the dehydration of glucose to 5-hydroxymethylfurfural (5-HMF) in a biphasic system. In this system, the parameters affecting the catalytic performance, such as CaCl_2 amount, reaction temperature and time, catalyst loading, volume ratio of water and methyl isobutyl ketone (MIBK), and reusability study were studied.

Chapter Five focuses the synthesis and characterization of LTL zeolite with different morphologies (short-rod, cylinder, stick and nanosize) using bamboo leaf ash (BLA) as silica source. Purely white BLA was first prepared and characterized before being used in the zeolite synthesis. The morphological effects on the porous properties and surface acidity of LTL zeolites were then examined using nitrogen adsorption-desorption measurement and pyridine adsorption analysis (Py-FTIR), respectively, before they were studied in the solvent-free acylation of 2-methylfuran with acetic anhydride reaction under non-microwave instant heating conditions.

Chapter Six reports a novel method in crystallizing hierarchical OFF zeolite using CTABr as an organic template. The effects of synthesis parameters such as crystallization time, heating time and reactants (SiO_2 , Al_2O_3 , K_2O , type of mineralizer, CTABr and H_2O) on the crystallization of OFF zeolite were studied. Furthermore, the catalytic behavior of synthesized OFF zeolite in the acylation of 2-methylfuran with acetic anhydride was investigated under non-microwave instant heating conditions.

Lastly, Chapter Seven is devoted to the conclusion of all the research findings. Suggestions for future works of this research are also proposed.

CHAPTER TWO

LITTERATURE REVIEW

2.1 Zeolites

Zeolites are aluminosilicate microporous materials composed of silica (SiO_4) and alumina (AlO_4) tetrahedra with O atoms connecting the neighbouring tetrahedral. In aluminosilicate zeolite, the framework is negatively charged due to the presence of Al^{3+} , and the non-framework cations are presence to neutralize the framework charge (Figure 2.1) [1,2].

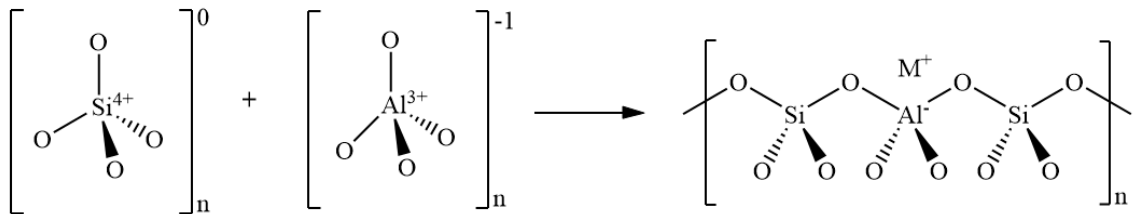
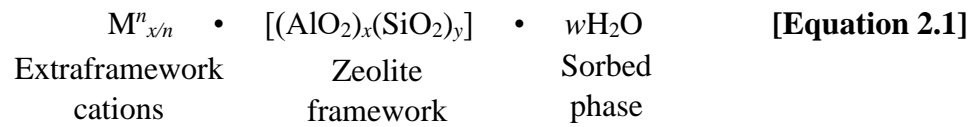


Figure 2.1. The formation of zeolite framework by of silica (SiO_4) and alumina (AlO_4) tetrahedra, where the metal cation (M^+) neutralizes the negative charged of aluminosilicate framework.

The non-framework cations can be exchangeable. The framework composition depends on the synthesis conditions [1,2]. The zeolite composition can be best described as having three components:



where M is generally a group I or II element such as sodium, potassium, cesium or magnesium. The variable n stands for the cation valance, x is equal or greater than 2, y is 2 to 10 and w is the number of water molecules in the structure of the zeolite [1,2].

The zeolite framework structure are made up of secondary building units (SBUs) that are built by the primary building units (PBUs) (TO_4 tetrahedra where T = Si or Al) [35]. The SBUs combine with each other to form different ring shapes such as single 4-, 6- and 8-rings (S4R, S6R, S8R), double 4-, 6- and 8-rings (D4R, D6R, D8R), polyhedral or complex units with cages and channels in different shapes [36]. Apart from PBUS and SBUs, zeolites are also made up of composite building units (CBUs) such as double rings, cancrinite cages and alpha cavities. CBUs are formed by a combination of rings, cages and channels where the size of the rings (4-, 5-, 6-, 8-, 10- and 12-MR) is determined by the number of Si and/or Al tetrahedra [37]. The SBUs and CBUs stacks up and form zeolite framework with unique pore size, shape and dimension.

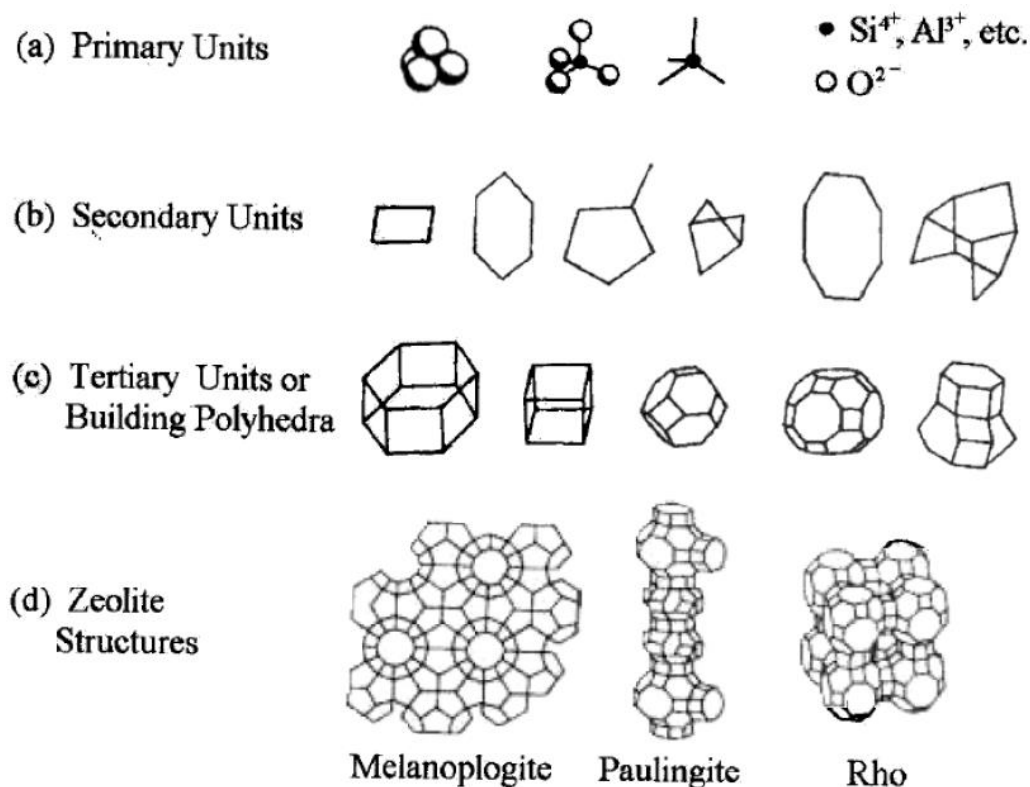


Figure 2.2. (a) Primary building units (PBUs), (b) secondary building units (SBUs), (c) tertiary units or composite building units (CBUs) and (d) zeolite structures [37].

2.2 History of zeolites

The zeolites history began in 1756 when a Swedish mineralogist Axel Fredrik Cronstedt discovered stilbite mineral [38]. He called it “zeolite” which derived from two Greek words, *zeo* (boil) and *lithos* (stone) because the mineral showed intumescence upon heating.

Since then, many researchers have investigated the properties of zeolite minerals (e.g. adsorption, cation exchangeability and dehydration) from 1777 to 1800s. The first hydrothermal synthesis of zeolite, levynite, was reported by St. Claire Deville in 1862 [39]. The idea proposing that the structure of dehydrated zeolites consists of

open spongy frameworks was first developed by Friedel in 1896 after seeing some organic molecules (alcohol, benzene and chloroform) were trapped by this porous materials [40]. In 1925, Weigel and Steinhoff reported the first molecular sieve effect after realizing chabazite zeolite can adsorb moisture, methanol, ethanol and methanoic acid without adsorbing acetone, ethers and cyclic compound. McBain then named these porous solid materials as “molecular sieve” [41].

The first use of X-ray diffraction for the identification in inorganic mineral synthesis was discovered by Leonard in 1927 [42]. Since then, Tylor and Pauling described the first single crystal structure of zeolite minerals in 1930 [43]. The first classification of zeolites using molecular size consideration was proposed by Richard M. Barrer in 1945 [44]. He also reported the first definitive synthesis of synthetic mordenite [45] and KFI-type zeolites [46]. The synthesis and discovery of zeolite use in adsorption had inspired Robert M. Milton and Donald W. Breck in discovering a number of commercially significant zeolites such as zeolite A, X and Y [47,48].

Up to now, around 250 types of zeolite have been successfully identified and approved by the International Zeolite Association (IZA) and they are assigned with a three-letter code such as ANA, LTJ, LTA, FAU, etc. based on the IUPAC Commission on Zeolite Nomenclature. Zeolites can be found naturally. Normally, the natural zeolites are of hydrothermally volcanic origin. They are also found in metamorphic rocks [48]. Natural zeolites usually have very small channel diameters due to structural impurities which disallow the adsorption of larger gas molecules and organic compounds [48]. On the other hand, synthetic zeolites are prepared in a controlled environment. These zeolites have very high purity, uniform pore distribution, large and tuneable pore sizes and shapes [49]. As a result, many synthetic zeolites, such as

zeolite Y, X and ZSM-5, have been widely synthesized and used in industries due to their distinct ion exchange, adsorption and catalytic properties.

2.3 Zeolite synthesis and formation

Various methods can be used to synthesize zeolites where hydrothermal process is the most common method in zeolite synthesis. It was first developed in the 1940s by Richard Barrer and Robert Milton [50]. Usually, the hydrothermal synthesis of zeolites involves the heating of a reactive hydrogel in an alkaline media at a temperature range between 80–220 °C under an autogenic pressure for a specific time [50]. The zeolite precursor suspensions typically contain water, silica and alumina sources, organic template and alkali earth metal cations (e.g. Na, K, or Cs). In the synthesis, the organic templates and metal cations serve as structure-directing agents (SDAs) where they help in the stabilization and formation of micropores in zeolite framework [50].

During crystallization process, an amorphous hydrogel is firstly formed by dissolving the silicate and aluminate sources in an inorganic/organic template solution (high pH) [50]. The polymerization and depolymerization of silicate and aluminate species (breaking and rebuilding the Si-O-T bonds (T = Si or Al)) occur concurrently in this step until it reaches an equilibrium phase [51]. The reactants remain amorphous until it reaches a certain period where zeolite starts to crystallize. At this point, the amorphous entities are then replaced by an approximately equal mass of crystalline zeolite phase. Finally, the pure zeolite crystals are formed and obtained. The resulting crystalline product is then recovered by proper washing and drying [50]. In some synthesis cases that use organic templates, they require an extra step of calcination

where the as-synthesized zeolite is heated at a very high temperature (normally 550 °C) in order to remove the occluded organic templates [52]. The entire synthesis of zeolite process is summarized in Figure 2.3.

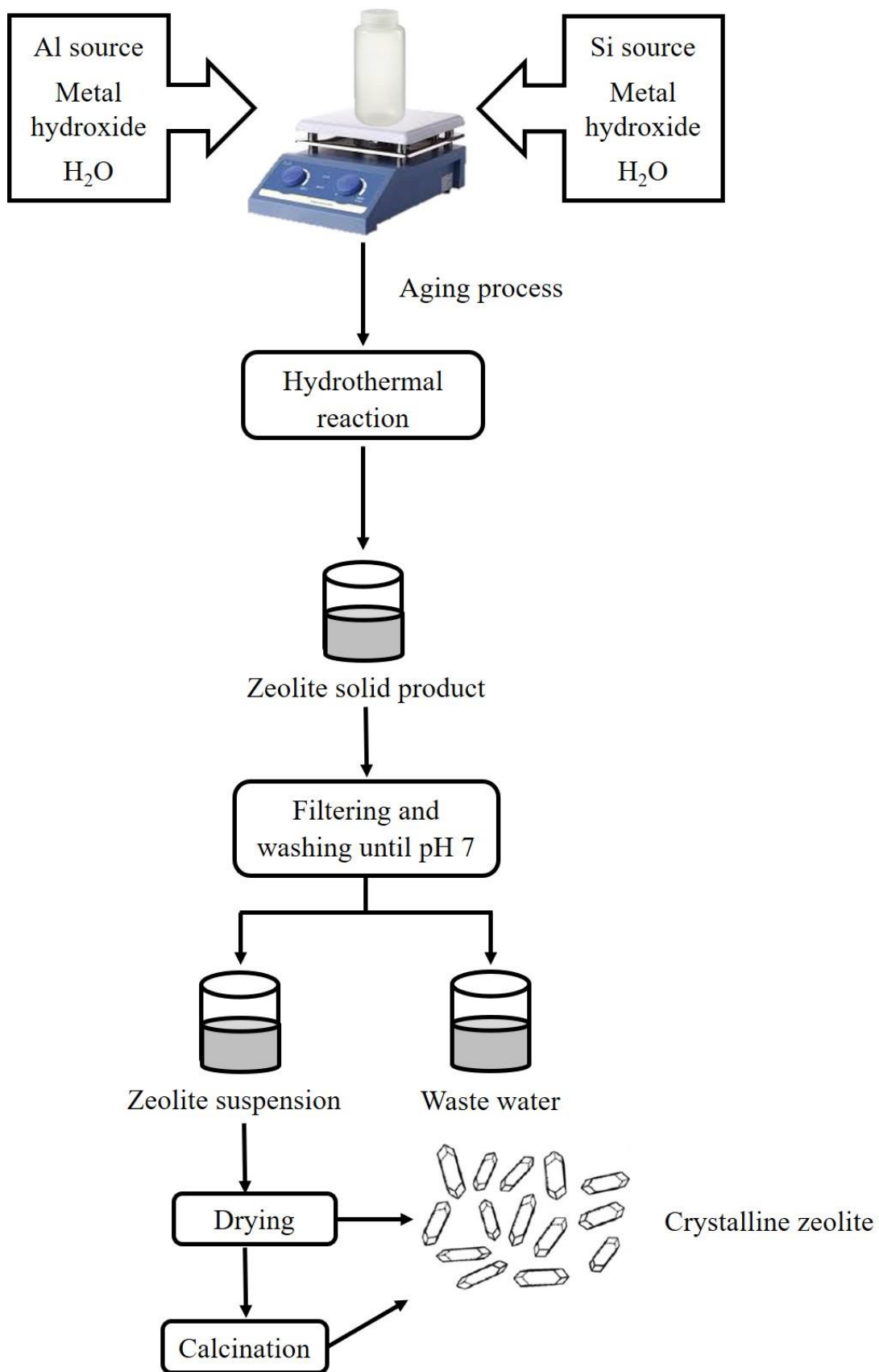


Figure 2.3. The hydrothermal process of zeolite synthesis.

In microscopic view, the zeolite formation involves several important stages. The process is initiated with the formation of discrete zeolite nuclei during the induction period. During this stage, supersaturation phenomenon occurs where the Si and Al sources undergo complete or partial dissolution of silica and alumina sources *via* condensation of oligomeric silicate and aluminate species. As a result, a clear or cloudy hydrogel suspension is formed [53]. The next step involves the growth of zeolite nuclei by consuming the nutrients from the mother liquor. The primary nucleation occurs either homogeneously or heterogeneously. Homogeneous nucleation is driven by the solution itself in the absence of foreign particles or crystals in the solution, while heterogeneous nucleation is induced by foreign particles in the solution [54]. The last step involves the crystal growth where small crystalline nuclei start to grow through a layer-by-layer mechanism. Sometimes, simultaneous secondary nucleation of another zeolite phase also happens at this stage [53]. It is because secondary nucleation has a lower activation energy than the primary nucleation where the second nucleation is induced by the parent crystals of the same phase. These particles may serve as seeds for the growth of second zeolite phase [54]. The relationship between the nucleation rate and the crystal growth can be summarised in Figure 2.4. According to Breck [55], zeolites are metastable species, and they will convert to more stable crystalline materials if they are kept heating in their synthesis magma. However, a detailed understanding on the formation of zeolite is still not achieved.

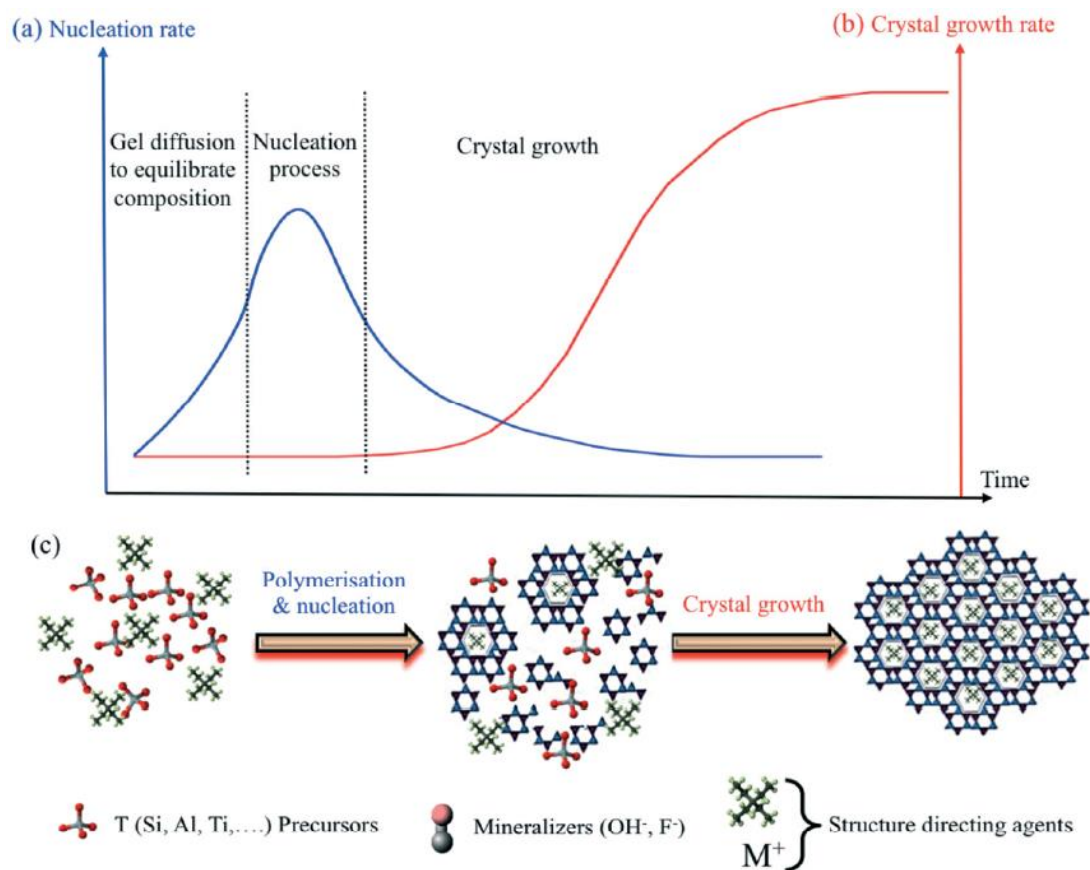


Figure 2.4. Schematic representation of the (a) nucleation and (b) crystal growth rate of zeolites, and (c) formation of zeolite from amorphous particles during the synthesis [56].

2.4 Effect of synthesis parameters on the formation of zeolites

There are numerous synthesis parameters influencing the formation of zeolites, including the source of silica and alumina, Si/Al ratio of precursor hydrogel, crystallization temperature and time, precursor alkalinity, mineralizing agents, water content, aging treatment and the presence of organic/inorganic template. All these parameters play an important role in determining the type, morphology, topology and properties of zeolites synthesized.

2.4.1 Source of silica and alumina

The type of silica and aluminum sources used can influence the overall zeolite products (e.g. particle size, crystal morphology). For instance, the surface area of silica source can affect the stability of nucleating centres that finally affect the purity of the zeolite [57]. The most commonly used silica sources are silica sol, fumed silica, sodium silicate, colloidal silica, amorphous silica and tetraethylorthosilicate (TEOS). There are also other silica sources reported such as raw powder glass [58], coal fly ash [59], volcanic glass [60] and kaolin [61]. Besides that, the silica in agricultural wastes such as rice husk [62], bamboo leaves [63] and sugarcane [64] have also been used in the zeolite syntheses.

Meanwhile, the widely used aluminum sources are aluminum hydroxide ($\text{Al}(\text{OH})_3$), aluminum foil, sodium aluminate (NaAlO_2), aluminum sulfate ($\text{Al}_2(\text{SO}_4)_3$), aluminum isopropoxide ($\text{Al}[\text{OCH}(\text{CH}_3)_2]_3$) and pseudoboehmite ($\text{AlO}(\text{OH})$). It was reported that the aluminate source used can influence the Si/Al ratio of the gel precursor, thus affecting the framework structure, degree of crystallinity and crystal growth of the zeolite products [65].

2.4.2 Effect of Si/Al ratio

The values of Si/Al ratio in precursor hydrogels can be modified from 1 to ∞ (pure siliceous). Tuning the concentration of Al might cause the distortion of Si-O-Al angle and bond length. Thus, it affects the nearby framework and non-framework atoms [66]. Generally, varying the Si/Al value results in the different concentrations and distributions of Si-O-Al species in zeolite structures [67]. Such arrangement leads to the alteration of the properties of zeolites [68]. The Si/Al ratio in zeolite precursors

influence their thermal stability, hydrophobicity/hydrophilicity, concentration and distribution of active sites and cation exchange capacity. When the Si/Al ratio decreases, the density of active sites and cation exchange capacity of the zeolite increase, thus leading to increased zeolite crystallinity [69,70].

2.4.3 Alkalinity

The synthesis of zeolites is generally performed under a basic condition where the degree of basicity depends on the molar ratio of OH^-/Si and $\text{M}_2\text{O}/\text{H}_2\text{O}$ ($\text{M} = \text{metal}$) of the hydrogel precursor. Zeolites are very rarely synthesized under acidic condition because high pH is needed to dissolve the Al and Si sources [71]. The alkalinity of a precursor gel controls the solubilization of Si and Al sources. The solubility of silicate and aluminate increases when the alkalinity increases. This leads to the acceleration of polymerization of the silicates and aluminates, and finally enhancing the induction and nucleation rates of zeolites [72]. As a result, zeolite crystals with smaller crystallite size and narrow particle size distribution are synthesized [73].

2.4.4 Effect of water content

Water is generally used as a solvent in the hydrothermal synthesis of zeolite. It is because it has the ability to dissolve most of the reactant and intermediate species in the precursor gel. Water also plays a role of structural directing agent as it is possible to steer the zeolite synthesis products by changing the concentration of the initial gel [74]. The amount of water in the synthesis system influences the type of framework formed as the crystallization process of different zeolites occurs within a narrow range

of pH [75,76]. In addition, the amount of water also affects the reactant concentration in the hydrogel solution, and it affects the size of the crystal and morphological properties of zeolites. By increasing the water content in the crystallizing system, the amount of the reactive species in the liquid is reduced, and hence decreasing the crystallization rate. The formation of zeolite crystals depends on the supersaturation of primary building units [77]. Thus, high concentration of reactant at low water content leads to an increase of alkalinity which in turn increases the supersaturation of the mother liquor. This condition promotes nucleation and hence producing small-sized crystal particles [78].

2.4.5 Effect of temperature synthesis

The crystallization temperature is one of the most important parameters in the synthesis of zeolite due to its strong influence in the nucleation, crystals growth rate and morphology properties of zeolites [79]. It also affects the zeolite purity since the purity is sensitive to a specific temperature range [80]. An increase in synthesis temperature will recrystallize a zeolite and transform it into other denser crystalline phases which are more thermodynamically and kinetically stable [81]. The synthesis temperature is directly proportional to the polymerization rate reaction between aluminate and silicate species [72]. As a result, both the nucleation and crystal growth rates are enhanced, forming larger crystals zeolite [82].

2.4.6 Effect of synthesis time

Heating time can affect the purity, morphology and crystallinity of a zeolite. In principle, the crystallinity increases with heating time. However, zeolites are thermodynamically metastable phases and according to Ostwald's law, a metastable phase would appear at the beginning and then is replaced by the more stable ones. For example, zeolite A (LTA), a metastable zeolite, is dissolved to form a more stable zeolite sodalite (SOD) with prolonged crystallization time [68]. Basically, increasing the crystallization time causes the dissolution of zeolites crystals in the alkaline solution, thus leading to the decrease of crystallinity [4]. As a result, a narrower size distribution of zeolites is observed with increasing the synthesis time. This is explained by the fact that the amorphous particles are converting into crystals and continues to grow as synthesis time is extended [5].

2.4.7 Effect of mineralizing agent

Mineralizer is a crucial component in the synthesis of zeolites as it enhances the dissolution of inorganic substances in the precursor gel forming a supersaturated solution by providing active species for nucleation and crystal growth of zeolites. The most commonly used mineralizers are hydroxide (OH^-) and fluoride (F^-) ions. The OH^- ions typically are applied in the synthesis of aluminum-rich zeolites which requires high pH environments [75]. The alkaline pH is adjusted by the addition of an inorganic or organic base where it is used as a template. Whereas, the F^- ion from ammonium fluoride (NH_4F), ammonium bifluoride (NH_4HF_2) or hydrogen fluoride (HF) are used as mineralizers for synthesizing siliceous zeolites (e.g. silicate-1) in a slightly acidic media (pH 5) [83]. It is observed that the morphological properties of

the zeolite crystals are affected by varying the mineralizer content [84]. When the mineralizer content increases, the average size of crystals reduces due to the enhancement of the solubility of aluminosilicate species in the precursor [85].

2.4.8 Effect of structure-directing agents (SDAs)

SDA is one of the components in a hydrogel precursor. In general, the porous networks in zeolites are directed and formed by a templating compound that can be eliminated after zeolite synthesis. SDAs are crucial for stabilizing the cavities (channels) to avoid collapse of the zeolite framework. Moreover, SDAs assist in the prevention of silica clusters aggregation, and thus favours the formation of intersections and channels [86, 87].

There are two types of SDA, alkali metal cations and organic cations. Alkali metal cations are normally added into the precursor hydrogel to control the pH. Thus, they show significant influences on the nucleation and crystallization of zeolites [53]. Alkali metal cations controls the formation of high-alumina zeolites due to their hydration spheres function [75]. It was reported that different cation species and its cation size may affect the zeolite crystallization process and favour the formation of a certain type of zeolite. For example, Ghrear et al [87] reported the synthesis of ABW zeolite by using cesium cation as inorganic SDA. However, when the cesium cation was substituted with sodium and potassium cation, zeolites with CAN and LTJ framework structures were synthesized, respectively. Besides, organic structure-directing agents (OSDAs) such as quaternary ammonium salts and amines are widely used in the synthesis of high-silica zeolite materials ($\text{Si/Al} > 10$) [75]. They give a templating effect that direct the formation of zeolite framework, often resulting in

zeolite with pure phases and smaller crystals with narrower particle size distribution. However, there are many drawbacks by using organic templates as SDAs, such as toxic and environmentally unfriendly, expensive, long crystallization time and low zeolite product yield [88]. Besides that, they also require an addition step of calcination where the zeolite products are burnt at high temperature to eliminate the OSDAs from the zeolite pores [45]. In some cases, the combination of inorganic and organic SDAs are applied so as to enhance the nucleation and crystallization rates of zeolites [75].

2.4.9 Effect of gel aging

Gel aging plays an important role in the synthesis of zeolites. It is a pre-crystallization step of the reaction mixture that occurs before the crystallization of zeolite synthesis. Generally, aging is a step of stirring the aluminosilicate hydrogels for a certain period of time at a temperature condition, either in room temperature [89] or higher temperature [90]. The subsequent step of zeolite crystallization occurs at a higher temperature than that for aging, and normally the crystallization time is shorter than that of conventional method without having aging treatment [89-91]. The aging step is usually used to enhance the crystallization, adjust the crystal size, and minimize impurities. When the hydrogel undergoes aging process, the nucleation rate is affected, thus leading to the reduction of induction and crystallization times [50]. This results in the decrease of crystal size, narrower crystal size distribution and increase in product yield [89].

2.5 Nanosized zeolites

Conventional synthetic zeolites are aluminosilicate crystalline solids composing of uniform microporosity (<2 nm). Nevertheless, a main limitation of zeolites is their microporous system that faces diffusion problems, which in turn causing catalyst deactivation by pore blockage and coke formation. Thus, the decrease in zeolite crystal size leads to the shortening of the diffusion path [3].

Nanosized particles with a crystallite size in the range of 5–100 nm have been a great interest in materials research due to their unique properties and hence, they are used in various applications such as catalysis, lubricant, sensing and so forth [3]. Typically, a decrease in zeolite crystal sizes causes an increment of external surface that will enhance some characteristics (e.g. surface polarity, hydrophilicity and surface reactivity). These enhance surface properties hence create new potentials for adsorbing and reacting bulk molecular species that are unable to diffuse through the zeolite micropores. The advantages of nanosized zeolites are shown in Figure 2.5.

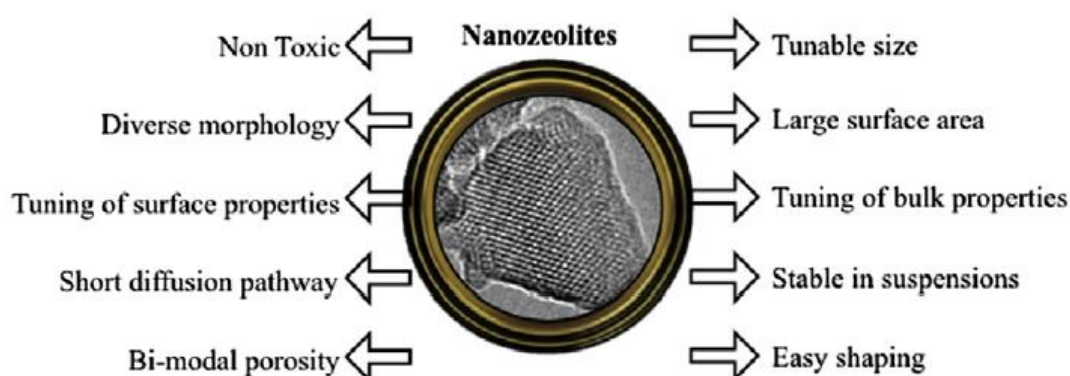


Figure 2.5. The properties of nanosized zeolites [3].

Nanosized zeolite with different morphologies and sizes can be synthesized by modifying the synthesis parameters (e.g. hydrogel composition, type of reactants used, crystallization time, synthesis technique and heating temperature). These parameters not only alter the nucleation process but also affect the crystal growth of nanozeolites [3]. The parameters influencing the formation of zeolite nanocrystals and the synthesis method are summarized in Figures 2.6 and 2.7, respectively. Currently, zeolite nanocrystals have extended their traditional applications (catalysis, adsorption and separation processes) to advanced applications such as thin films, membranes, sensors, optics, biomedicine, pharmaceutical area, cosmetic and agriculture [92].

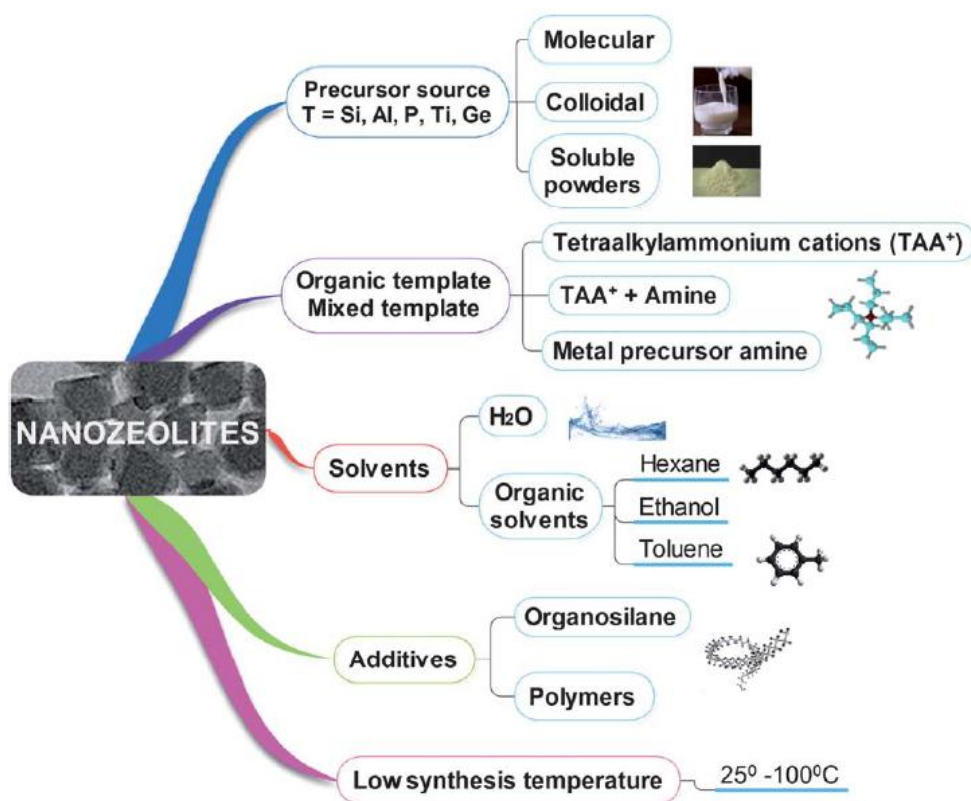


Figure 2.6. Synthesis parameters affecting the formation of zeolite nanocrystals [92].

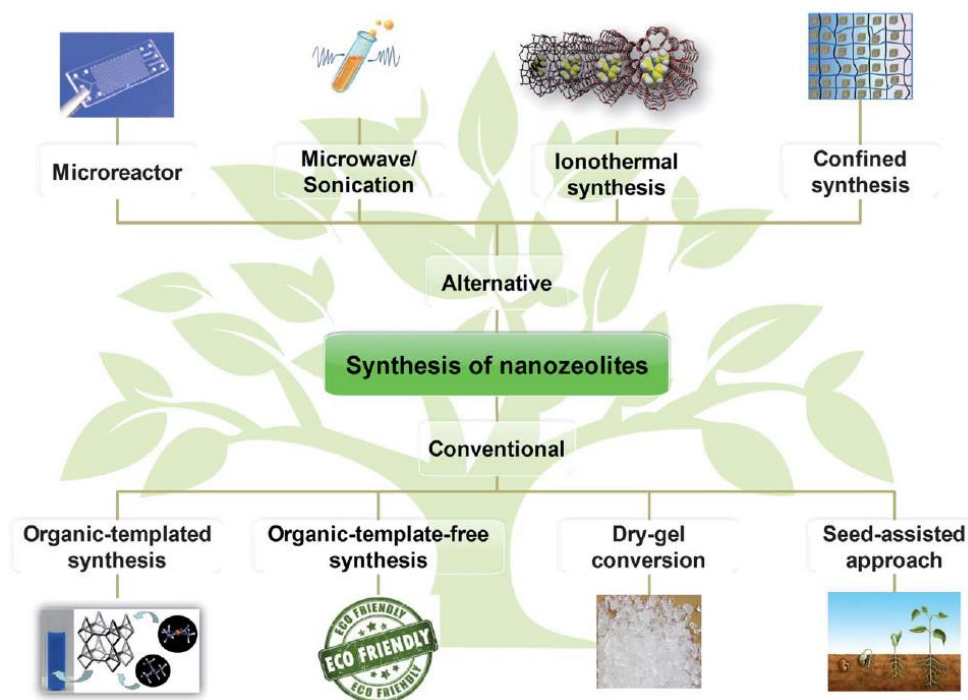


Figure 2.7. The synthesis methods of nanosized zeolites [92].

2.6 Hierarchical zeolites

Zeolites with larger micropores can minimize the diffusion limitation by reducing the intracrystalline diffusion path length. In addition, this can also be achieved by decreasing the zeolite crystal, thus enhancing the catalyst effectiveness [93-99]. In general, it is more favourable to synthesize a material with secondary pore system consisting of mesopores (2-50 nm) inside the microporous zeolite crystal. Such solids are commonly named as hierarchical porous materials [100,101]. The hierarchical porous materials have various porosities (micropores, mesopores and macropores). Micropores and mesopores are good for the molecular size and shape selectivity, while macropores improve the molecular diffusivity and accessibility which eliminate the diffusion restriction for large molecules of reactants and products [102]. Figure 2.8